SHARAD sounding radar on the Mars Reconnaissance Orbiter

Roberto Seu,[1] Roger J. Phillips,[2] Daniela Biccari,[1] Roberto Orosei,[3] Arturo Masdea,[1] Giovanni Picardi,[1] Ali Safaeinili,[4] Bruce A. Campbell,[5] Jeffrey J. Plaut,[4] Lucia Marinangeli,[6] Suzanne E. Smrekar,[4] and Daniel C. Nunes[7]

Received 7 May 2006; revised 22 September 2006; accepted 19 October 2006; published 18 May 2007.

[1] SHARAD (SHAllow RADar) is a sounding radar provided by Agenzia Spaziale Italiana (ASI) as a Facility Instrument on the Mars Reconnaissance Orbiter mission. Its 20-MHz center frequency and 10-MHz bandwidth complement the lower-frequency, relatively narrower bandwidth capability of the MARSIS sounding radar. A joint Italian-U.S. team has guided the experiment development and is responsible for data analysis and interpretation. The radar transmits signals at a 700 Hz pulse repetition frequency (PRF) and collects reflections from both the surface and near subsurface of Mars. Vertical and horizontal resolutions are, respectively, 15 m (free-space) and 3–6 km (cross-track) by 0.3–1 km (along-track). The scientific objective of SHARAD is to map, in selected locales, dielectric interfaces to at least several hundred meters depth in the Martian subsurface and to interpret these results in terms of the occurrence and distribution of expected materials, including competent rock, soil, water, and ice. A signal-to-noise ratio of ~50 dB (for a specular surface return) is achieved with 10 W of radiated power by using range and azimuth focusing in ground data processing. Preprocessed data as well as range- and azimuth-focused data will be formatted according to Planetary Data System (PDS) standards and be made available from the ASI Science Data Center (ASDC) and from the Geosciences Node of the Planetary Data System (PDS). Important targets for SHARAD include the polar layered deposits, sedimentary stacks (especially in Terra Meridiani), buried channel systems, buried impact craters, volcanic complexes, and shallow ice deposits in equilibrium with the atmosphere.

Citation: Seu, R., et al. (2007), SHARAD sounding radar on the Mars Reconnaissance Orbiter, *J. Geophys. Res.*, *112*, E05S05, doi:10.1029/2006JE002745.

1. Introduction

1.1. Experiment Overview

[2] Exploration from orbit and by rovers shows that Mars has undergone dramatic shifts in its climate and geologic regime over time. The most important of these is the transition from an epoch of abundant surface water after the end of heavy bombardment to a cold, dry environment. In this transition, much of the surface water was trapped as polar caps, circum-polar layered deposits, and extensive ground ice. The record of changing climate and geologic processes is preserved in the subsurface as layering associated with water-deposited sedimentary rocks, volcanic sequences, and the seasonal and long-term obliquity-driven movement of volatiles. Orbital remote sensing that probes to depths of hundreds of meters to kilometers offers the only practical means for studying such layering over large areas.

[3] Electromagnetic remote sensing typically probes to greater depths in a target medium as the illuminating wavelength increases (frequency decreases). To penetrate typical near-surface crustal materials and characterize layers at significant depth, the active signal must have a wavelength of several meters or more. Radio echo (radar) sounding is a technique that has been shown to reveal subsurface layers when used at the surface of the Earth (Ground Penetrating Radar), from aircraft, and from orbit around the Moon [*Peeples et al.*, 1978]. Radar sounding at frequencies of tens to a few hundred MHz has been used to study the subsurface characteristics of the Earth's ice sheets, which can be many kilometers in thickness [e.g., *Holt et al.*, 2006a].

[4] The SHARAD (SHAllow RADar) radar sounder provided by Agenzia Spaziale Italiana (ASI), now in orbit aboard the Mars Reconnaissance Orbiter (MRO) [*Zurek and Smrekar*, 2007], is designed to detect dielectric contrasts

[1]INFOCOM, Università di Roma "La Sapienza," Rome, Italy.
[2]Department of Earth and Planetary Sciences, Washington University, St. Louis, Missouri, USA.
[3]Istituto di Astrofisica Spaziale e Fisica Cosmica, Rome, Italy.
[4]Jet Propulsion Laboratory, California Institute of Technology, Pasadena, California, USA.
[5]Center for Earth and Planetary Studies, Smithsonian Institution, Washington, D. C., USA.
[6]IRSPS, Università G. d'Annunzio, Pescara, Italy.
[7]Lunar and Planetary Institute, Houston, Texas, USA.

0148-0227/07/2006JE002745

Table 1. SHARAD Team Members

Team Member	Role/Responsibility	Institution
Roberto Seu	Team Leader/Radar Performance and Data Processing	Università di Roma "La Sapienza"
Roger Phillips	Deputy Team Leader/Mission Science Strategy and Interpretation	Washington University in St. Louis
Daniela Biccari	Mission Operations	Università di Roma "La Sapienza"
Roberto Orosei	Data Products	IASF, Istituto Nazionale di Astrofisica
Ali Safaeinili	Instrument Scientist	Jet Propulsion Laboratory
Arturo Masdea	Calibration and Commissioning	Università di Roma "La Sapienza"
Costanzo Federico	Data fusion and GIS	University of Perugia
Vittorio Formisano	Science Interpretation	Istituto di Fisica dello Spazio Interplanetario
Pierfrancesco Lombardo	Science Interpretation	Università di Roma "La Sapienza"
Lucia Marinangeli	Mission Science Targeting; E/PO	Università d'Annunzio
Giovanni Picardi	Surface Cutter Models; MARSIS	Università di Roma "La Sapienza"
Sebastiano B. Serpico	Science Interpretation	Università di Genova
Bruce Campbell	Clutter Detection and Mitigation	Center for Earth and Planetary Studies, Smithsonian Inst.
Jeffrey Plaut	MARSIS Correlation	Jet Propulsion Laboratory
Suzanne Smrekar	Science Interpretation	Jet Propulsion Laboratory

associated with geologic layering on vertical scales of 15 m or better and to probe to typically subkilometer depths. SHARAD will complement the spatially coarse, but deep sounding of the MARSIS instrument on Mars Express [*Picardi et al.*, 2005] (see section 2.2). The SHARAD radar emits electromagnetic (EM) waves from its 10-m dipole antenna, and measures the reflections from both the Martian surface and subsurface. Waves that are transmitted into the subsurface may reflect from dielectric interfaces and return to the instrument at greater time delay than the surface echo. A two-dimensional picture (a "radargram") of the surface and subsurface is built up in one direction by time delay and in an orthogonal direction by motion of the MRO spacecraft (S/C) along its orbit (see Figures 3, 4, and 8). The primary obstacle to the identification of subsurface echoes is the interference from off-nadir surface echoes (known as "surface clutter") that arrive at the radar receiver with the same time delay as subsurface echoes. This can be mitigated by various methods discussed in section 8.

[5] SHARAD operates with a 20-MHz center frequency and a 10-MHz bandwidth, which translates to a vertical resolution of 15 m in free-space and $15/\sqrt{\varepsilon}$ m in a medium of relative permittivity ε. The transmitted signal is a 10 W, 85-μsec chirped (linear FM) pulse emitted from a 10-m-long dipole antenna that is used for both transmitting and receiving. Horizontal surface resolution depends on surface roughness characteristics, but for most Mars surfaces the cross-track footprint is 3–6 km and the along-track footprint, narrowed by synthetic aperture processing on the ground, is 0.3–1 km. The returned signal is recorded as a time series of complex-valued voltages. The pulse repetition frequency (PRF) over-samples the Doppler spectrum, allowing for coherent integration of pulses on board the spacecraft, while still allowing for Doppler focusing in ground data processing. Indeed, except for onboard presumming, all of the data processing will take place on the ground, including range and Doppler focusing of the chirp signals, and calibration of the processed data.

[6] Data will be processed at the SHARAD Operations Center (SHOC) of Alcatel Alenia Spazio (AAS) in Rome, Italy, under contract to ASI and under the guidance and control of the SHARAD science team. Data will be distributed to the community at large from the ASI Science Data Center (ASDC) in Frascati, Italy, and from the Geosciences Node of the Planetary Data System at Washington University in St. Louis, USA (WUSTL-PDS).

[7] The Italian portion of the SHARAD team was originally appointed by ASI, with Roberto Seu of Università di Roma "La Sapienza" as the Team leader. Subsequently, three American scientists were selected by NASA in response to an AO, with Roger Phillips of Washington University appointed Deputy Team Leader. US Participating Scientists likely will be added to the team. The full list of team members is given in Table 1, and includes Ali Safaeinili, the Instrument Scientist at JPL. The SHARAD team provided the instrument requirements to the prime contractor, AAS, and closely monitored the development of the hardware to ensure that the requirements were met.

[8] A review of the SHARAD radar experiment with an emphasis on its design is given by *Seu et al.* [2004].

1.2. Scientific Objectives

[9] The primary objective of the SHARAD experiment is to map, in selected locales, dielectric interfaces to several hundred meters depth in the Martian subsurface and to interpret these results in terms of the occurrence and distribution of expected materials, including competent rock, soil, water and ice [*Seu et al.*, 2004]. This is a seemingly cautious set of objectives, making no particular promises about the unique detection of any specific material (e.g., water). Nevertheless, the subsurface of Mars presents ample possibilities for dielectric contrasts. The dielectric constant depends on both rock porosity and rock composition, so boundaries between materials with differences in these properties are dielectric reflectors. This dielectric contrast could arise, for example, from sedimentary materials in contact with basaltic rock, from ice in contact with solid rock, or from ice-saturated porous rock in contact with ice-free porous rock. These contrasts alone lead to a large variety of subsurface targets for SHARAD to map. Examples include mapping of (1) the polar layered deposits, both their internal layers and contact with underlying bedrock, (2) the layering within sedimentary rock sequences, (3) buried impact craters in the northern lowlands, (4) buried channels,

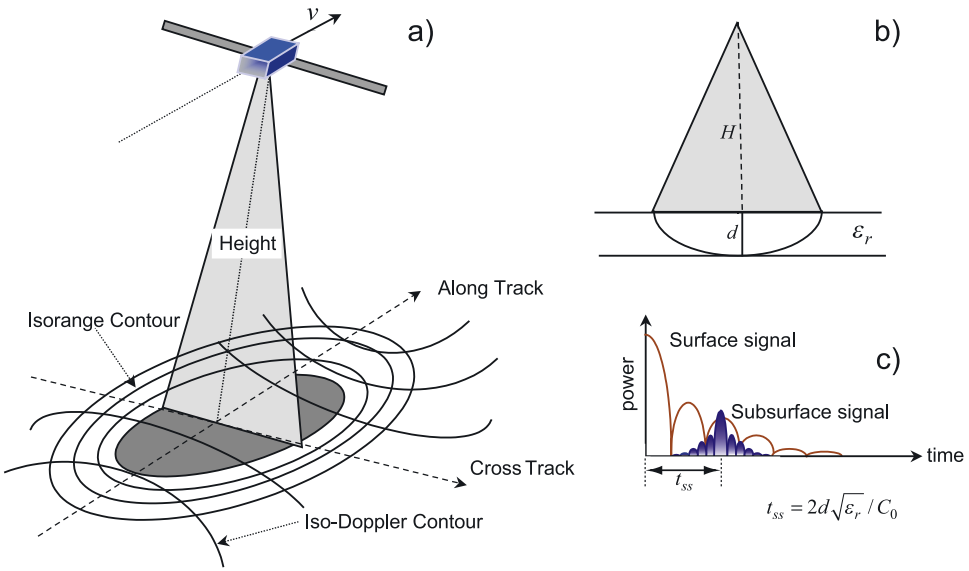

Figure 1. Principle of operation of a radar sounder. (a) Ground resolution is a function of range to surface (cross-track) and Doppler shift of returned signal (along-track). (b) Hypothetical example of subsurface reflector at depth d and passing through material of real dielectric constant ε_r. (c) Hypothetical radar trace showing weak subsurface signal in the presence of a strong surface return. The subsurface reflection is slightly stronger than the sidelobes (at the same time delay) associated with the surface reflection.

(5) volcanic stratigraphy, (6) shallow ice bodies, and (7) potential shallow water accumulations.

2. Radar Sounding

2.1. Principles

[10] The basic principles of radar sounding are straightforward and are sketched in Figure 1. The radar transmitter generates a high-power pulse, which is radiated by the antenna toward the Martian surface. As discussed in the Introduction, the surface will reflect some of the energy back toward the sounder, typically with a strong "quasi-specular" behavior due to mirror-like reflections from parts of the surface tilted toward the sensor [*Hagfors*, 1964]. Some of the energy impinging on the surface will be transmitted to the subsurface and will then travel toward the next reflecting interface, undergoing attenuation by the material as it propagates. When this signal encounters the second dielectric interface, some of it will be returned toward the sounder and the remainder will be transmitted further downward. In principle, due to transmission and attenuation losses, the returns from the subsurface should be much weaker than those of the surface.

[11] In order to transmit enough energy from the antenna to the surface, the transmitted waveform must be spread over a much longer period than that which corresponds to the desired time resolution. The longer pulse must then be "compressed" after reflection to recover the desired resolution and to isolate weak subsurface returns that are close to the strong surface echo. SHARAD employs a linearly-varying, frequency-modulated signal, or "chirp," to achieve small effective pulse lengths with adequate incident power. This use of a linear frequency modulated signal can, however, produce sidelobes that limit the subsurface detection capability of the radar (e.g., Figure 1c).

[12] The first observed echo is the strong return from the surface, which decays rapidly with time delay. Topographic features away from the nadir track will contribute unwanted "clutter" power at longer delays. The strength of subsurface returns generally decreases as the depth of the reflecting interface increases, until finally the signals are lost in a combination of surface clutter and/or cosmic radio noise. The detection of an isolated subsurface feature is therefore dependent upon the strength of that particular subsurface return clearly rising above both the overall noise level of the system and the level of near-nadir and off-nadir surface returns arriving at the same time.

[13] Therefore, to assess the expected performance of a Martian radar sounder, all of the following factors must be evaluated:

[14] 1. The reflectivity of the surface and the subsurface as a function of the expected material composition and interface characteristics.

[15] 2. The effect of the ionosphere. A Martian-orbiting radar sounder operating at a frequency of few MHz can expect a significant drop in performance due to the ionosphere, while even in the SHARAD frequency range (15–25 MHz) there will be some effects during daytime sounding.

[16] 3. The level of noise from the receiver system and the background environment.

[17] 4. The level of clutter echoes, which in turn are dependent on the surface topography.

[18] An example of the behavior of sounder echoes is shown in Figure 2 [*Peeples et al.*, 1978] and is based on the data taken by the Apollo Lunar Sounder Experiment, a pioneering sounder operated on board the Apollo 17 Command and Service Module in 1972.

[19] The first surface reflection echoes of the sounder can be also processed to give estimates of the average height, roughness and reflection coefficient of the surface layer by

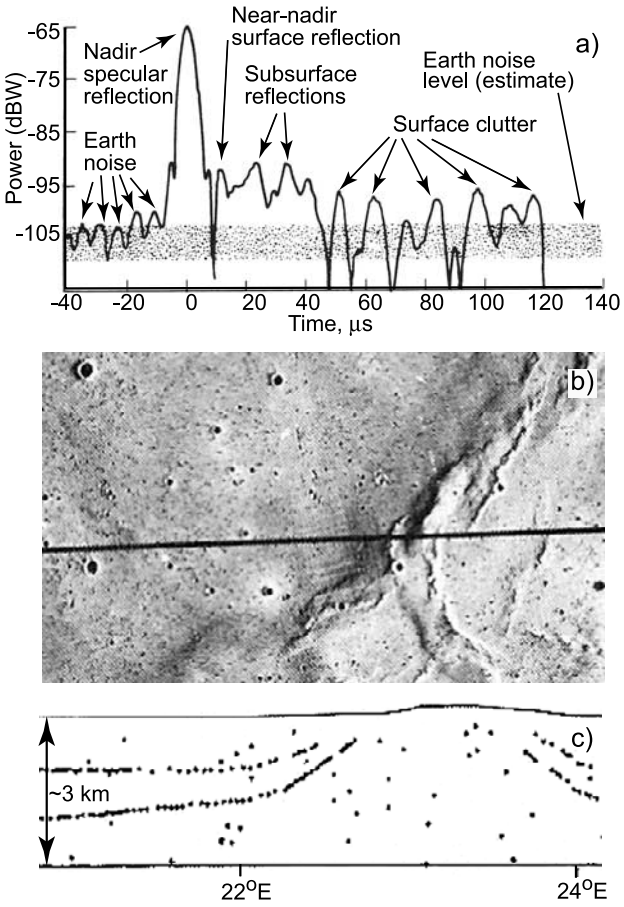

Figure 2. Sounding radar results from the 5-MHz channel on the Apollo Lunar Sounder Experiment (ALSE) on Apollo 17 [modified from *Peeples et al.*, 1978]. (a) Example echo power versus time from digital SAR processing. (b) ALSE ground track over the southeastern portion of Mare Serenitatis. (c) Corresponding subsurface sounding results. Black dots represent radar returns that did not have stereo separation between two adjacent parallel orbital tracks. These are interpreted as subsurface interfaces at ~900 and ~1600 m depth that have been disturbed by reverse faulting manifested at the surface by a wrinkle ridge.

using a classical altimetric approach (surface altimetry). The time delay of the echo makes it possible to estimate the average distance of the radar return from a reference surface level (e.g., the areoid), while the shape of the waveform provides information about the large-scale surface roughness averaged over the pulse-limited spatial resolution cell [*Hagfors*, 1964]. Finally the peak and/or time-integrated value of the average echo waveform can be used to estimate the backscattering coefficient and Fresnel reflection coefficient of the surface [cf. *Ford and Pettengill*, 1992].

2.2. SHARAD and MARSIS

[20] SHARAD was preceded at Mars by a lower-frequency radar sounder known as MARSIS, the Mars Advanced Radar for Subsurface and Ionospheric Sounding [*Picardi et al.*, 2004], on the European Space Agency Mars Express orbiter. MARSIS was designed for maximum subsurface penetration depths and thus uses frequencies as low as possible, given the Mars environment (particularly the ionosphere) and the constraints of hardware implementation. For subsurface sounding, MARSIS utilizes four frequency bands, each of 1 MHz bandwidth, centered at 1.8, 3.0, 4.0 and 5.0 MHz. Data may be collected with any two of the four frequencies simultaneously. A second mode is available for ionospheric sounding, using a series of pulses in frequency steps from 0.1 to 5.5 MHz. The basic properties of both the SHARAD and MARSIS radars are given in Table 2.

[21] One of the first major findings reported from the MARSIS experiment was the detection of the base of the North Polar Layered Deposits (NPLD), as shown in Figure 3 [*Picardi et al.*, 2005]. At 5 MHz, the MARSIS signals easily penetrated the 1.8 km of NPLD materials. The strength of reflections from the interior boundary indicates that the NPLD materials do not appreciably attenuate the signal, and the authors concluded that they consist of nearly pure ice, with no more that a few percent impurities present. *Picardi et al.* [2005] considered a simple two-layer model to interpret the ~10 dB loss in the signal from the subsurface boundary relative to the surface reflection for the 5-MHz MARSIS signal. The power of the subsurface signal is given by

$$\Gamma_{SS} = R_{12}^2\left(1 - R_{01}^2\right)^2 \exp\left[\left(-4\pi f\sqrt{\mu\varepsilon_0}\sqrt{\varepsilon_r}\tan\delta\right)d\right], \quad (1)$$

Table 2. SHARAD and MARSIS Instrument Parameters

	SHARAD	MARSIS
Frequency band	15–25 MHz chirp	1.3–2.3 MHz, 2.5–3.5 MHz, 3.5–4.5 MHz, 4.5–5.5 MHz chirps
Vertical resolution, theoretical, reciprocal bandwidth, $\varepsilon_r = 4$	7.5 m	75 m
Transmitter power	10 W	10 W
Pulse length	85 μs	250 or 30 μs
PRF	700/350 Hz	127 Hz
Antenna	10-m tip-to-tip dipole	40-m tip-to-tip dipole
Postprocessor SNR (worst-best)	50–58[a] dB	30–50[b] dB
Horizontal resolution (along track × cross track)	0.3–1 km × 3–6 km	5–10 km × 10–30 km

[a]Estimate.
[b]Actual.

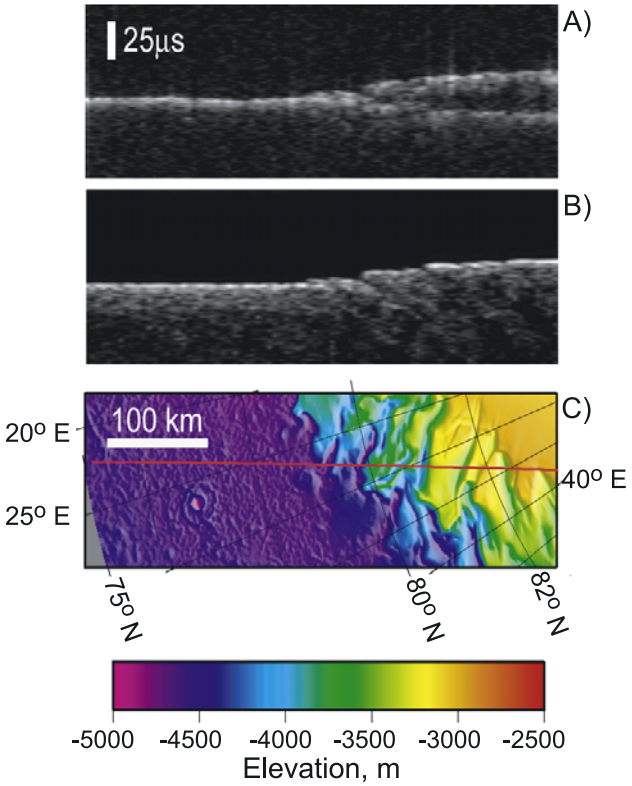

Figure 3. (a) MARSIS data in radargram format for orbit 1855 as it crosses the margin of the North Polar Layered Deposits. (b) Simulated MARSIS data if echoes are only from the surface (nadir and off-nadir clutter). (c) MOLA topography along the ground track (red line); elevation is relative to mean planetary radius. MARSIS data at 5 MHz show a split of the strong return into two as the ground track reaches the layered deposits (higher terrain to the right). Maximum time delay to the second reflector is 21 μs, equivalent to 1.8 km depth in water ice. Adapted from *Picardi et al.* [2005].

where R_{12} is the reflection coefficient at the subsurface interface, R_{01} is the reflection coefficient at the surface interface, f is frequency, μ is magnetic permeability (taken here as the free-space value, μ_0), ε_0 is the permittivity of free space, ε_r is the real part of the dielectric constant (relative permittivity) of the propagation medium (here the NPLD), tanδ is the ratio of the imaginary part (ε_i) of the dielectric constant to ε_r in the medium, and d is the depth to the subsurface interface. If the real parts of the dielectric constants in the NPLD and an assumed underlying basaltic regolith are 3 and 4.5, respectively, then interface (transmission) loss accounts for more than 9 dB of the ~10 dB of total relative loss. Path loss (the exponential part) accounts for about 0.6 dB of loss in the model and according to equation (1) is logarithmically proportional to frequency. The SHARAD center frequency (20 MHz) is four times greater than the 5-MHz MARSIS signal, so a path loss of about 2.4 dB and a total loss of ~12 dB is predicted. This is conservative, as some of the path loss is actually frequency-independent interface loss at the many internal layers in the NPLD, which are not accounted for in this simple model. This analysis suggests that the SHARAD signal will penetrate almost as deeply as the MARSIS signal in the Polar Layered Deposits (but with an order of magnitude better vertical resolution). This conclusion is bolstered by MARSIS results indicating that the highest-frequency bands penetrated just as deeply as the lower-frequency bands.

[22] *Picardi et al.* [2005] also reported the apparent detection of a 200–300 km diameter circular structure in the shallow subsurface of the northern lowlands Chryse region, which they interpreted as a buried impact basin (Figure 4). A bright horizontal reflector was seen at a time delay corresponding to a depth of 2–2.5 km. Again, the

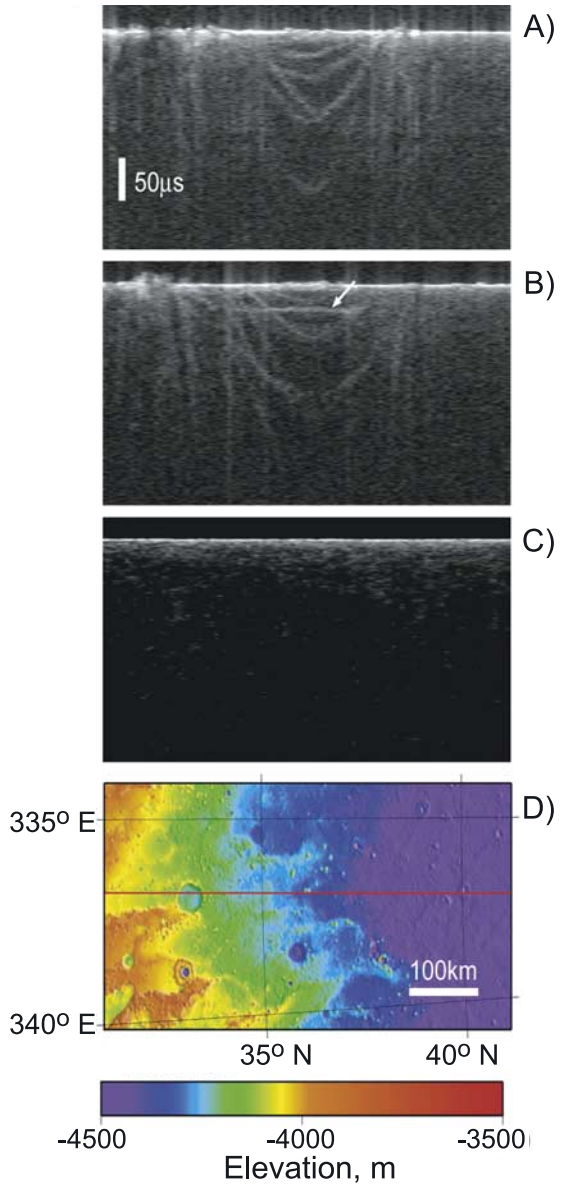

Figure 4. MARSIS data for orbits (a) 1892 (3 MHz band) and (b) 1903 (4 MHz band). Note the multiple arc-shaped reflectors near the center of each panel and the planar reflector associated with the arcs in orbit 1903 (arrow). (c) Model of the nadir surface and off-nadir clutter for orbit 1903. No arc-like or planar features are predicted in the clutter model. (d) MOLA topography along the ground track of orbit 1903. Adapted from *Picardi et al.* [2005].

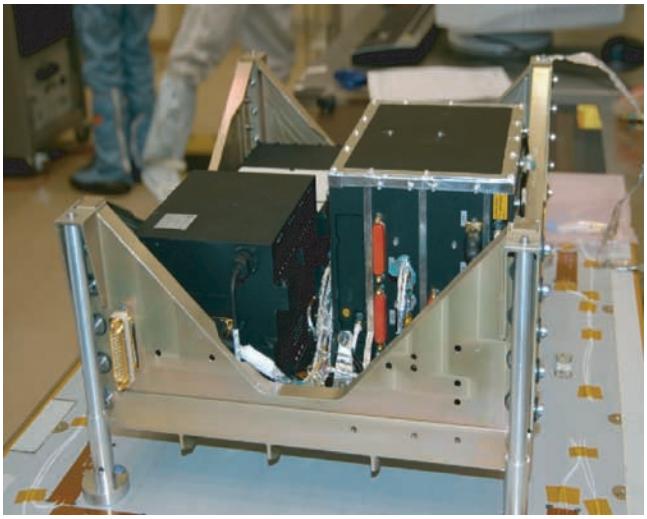

Figure 5. SHARAD Electronics Box (SEB).

strength of the subsurface reflection implied only minor losses in the intervening layer, suggesting the nonunique possibility of ice-rich material filling the basin to several km depth. The detailed structure of the hypothesized basin may be revealed by SHARAD, which may also be useful in augmenting the inventory of proposed buried impact features that MARSIS subsequently discovered [*Watters et al.*, 2006].

[23] More recently, MARSIS has detected fine layering within the South Polar Layered Deposits (SPLD) [*Plaut et al.*, 2006]. The higher vertical resolution of SHARAD should allow much better discrimination of this layering, providing additional insight into the compositional or physical variations responsible for the observed dielectric layering. Shallow (several 100s of m) interfaces have been detected by MARSIS in areas adjacent to the classical mapped SPLD [*Plaut et al.*, 2006]. These shallow deposits, likely ice-rich, are prime targets for SHARAD. In lower latitudes, MARSIS has detected shallow interfaces that should be detectable with SHARAD at better resolution. The so-called ''Stealth'' materials and related units of the Medusae Fossae formation, which display subsurface interfaces in MARSIS data [*Ivanov et al.*, 2006], will also be important targets for SHARAD.

3. Instrument Description

[24] SHARAD is composed of two main physical elements, the SEB (SHARAD Electronics Box) and the antenna. The SEB includes all of the transceiver electronics and the signal processing and control functions. It is made up of two separate electronic assemblies (RDS and TFE) mounted on a support structure that acts as radiator for thermal control and includes the heaters and temperature sensors.

[25] The Receiver and Digital Section (RDS) is, in turn, divided into (1) the DES (Digital Electronic Section), which carries out instrument control, communication with the spacecraft (S/C), timing generation, postprocessing of the received data, and generation of the transmitted chirp signal; and (2) the Receiver (Rx), which amplifies, filters and digitizes the received signal. The TFE (Transmitter and Front End) provides amplification of the transmitted signal, transmitter/receiver (Tx/Rx) duplexing, and includes the matching network required to interface with the antenna. The proto-flight model of the SHARAD Electronics Box is shown in Figure 5.

3.1. Transmitter/Front-End

[26] The Transmitter & Front End Unit (TFE) is a self-standing component, devoted to amplifying the low level chirp signals coming from the DES unit and coupling them to the dipole antenna; the unit also provides for the time division duplexing function, i.e., sharing the antenna between the transmitter and the receiver path. The TFE includes an internal DC/DC converter to supply all internal circuitry and to provide galvanic isolation from the power bus; the power supply assures high peak energy over the pulse duration, while preventing both excessive current transients on the main bus and ripple on the secondary voltage rails.

[27] The main feature of the TFE is the capability of handling wide-bandwidth frequency modulated pulsed signals (15–25 MHz), while minimizing the amplitude/phase distortions (in spite of the fact that the highly-mismatched antenna load causes significant amplitude and phase ripples over the useful bandwidth). The TFE performance, especially the output power, is very dependent on the impedance characteristics of the antenna, which represents the output load of the radar. A dummy load reproducing the antenna was designed and implemented for testing purposes.

3.2. Receiver

[28] From an architectural point of view, SHARAD's receiver has been designed without the need for frequency conversion; the receiver's front end performs a band-pass filtering function, while the received signal is amplified to a level sufficient for A/D (analog to digital) conversion. The SHARAD receiver is based on a band-pass sampling technique, so the sampling rate can be much lower than that required by sampling at twice (or more) the highest-frequency content of the band-pass signal. In fact, to satisfy Nyquist's theorem, the sampling rate must be at least twice the bandwidth of interest, not necessarily twice the highest-frequency component. The choice of direct digitization of the RF input signal has, for this application, several advantages with respect to a frequency-conversion configured receiver. The most obvious reason is that a conversion mixer is not required. A built-in local oscillator for conversion is also not needed.

3.3. Digital Subsystem

[29] The Digital Electronics Section (DES) is the heart of SHARAD and contains many of the instrument functions, including command and control, low-power radar pulse generation, science data processing and formatting, and timing. The DES provides all the hardware and software components to enable SHARAD operations. These components are used to perform the following functions:

[30] 1. Command and control capability (by way of S/C's command and data handling system).

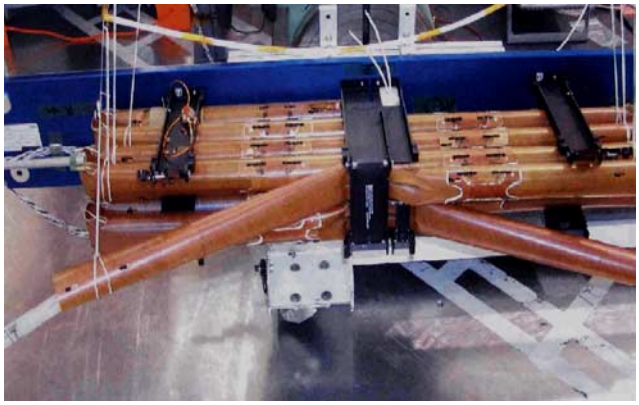

Figure 6. Folded SHARAD Antenna during a deployment test.

[31] 2. Command and control capability of other SHARAD units.

[32] 3. Formatting of science data and their transfer as telemetry to the S/C's solid state recorder (SSR).

[33] 4. Generation of housekeeping telemetry and its transfer to the S/C's SSR.

[34] 5. Generation of the radar chirp signal.

[35] 6. Processing of raw radar data.

[36] 7. Provision of a high-stability oscillator and generation of timekeeping and synchronization signals for all SHARAD units.

[37] 8. Power conditioning and distribution to the other SHARAD units.

[38] The DES is based on a modular design, and the receiver section (Rx) shares the same mechanical form factor as the DES and is joined to it. The DES is composed of the following items:

[39] 1. Digital Signal Processor (DSP) Module (Command and Control Board and Slave board).

[40] 2. Service Module (Timing Board and DC/DC Converter board).

[41] 3. Digital Chirp Generator (DCG) Module (DCG board).

[42] 4. Harness.

[43] 5. Mechanics.

[44] The components of each module are mounted on their own mechanical frame. The boards are connected to one another through the DES internal harness, which also allows the connections with the SHARAD Receiver.

[45] Digital Chirp Generator: The Digital Chirp Generator (DCG) is a module that synthesizes the chirp signals in the Digital Electronic Section (DES). It has been designed using the Direct Digital Synthesis technique, which consists of the generation of discrete samples of a sine wave at different frequencies and the successive reconstruction of the desired waveform at the analog level. A custom Numerical Controlled Oscillator (NCO) has been employed to implement this technique. The NCO allows savings in both surface area and power consumption. The DCG is a programmable signal generator. This characteristic allows SHARAD to achieve a high flexibility and adaptability during the mission. The NCO is implemented on a single fully space-qualified Application-Specific Integrated Circuit (ASIC). The main features of the NCO are as follows:

[46] 1. Flexibility: All parameters are configurable (start frequency, frequency slope, phase compensation, pulse duration).

[47] 2. Frequency Resolution: 32-bits (0.018 Hz @ 80 MHz clock).

[48] 3. Wide Output Bandwidth: 0 to 32 MHz @ 80 MHz clock.

[49] 4. CW or Chirp Signal Gen.: 10 bit outputs.

[50] 5. Automatic Download of the External Look-up Table PROM content.

[51] 6. μProcessor Compatible Input (16 bits Bus Address and 16 bits Bus Data).

[52] 7. Low Power Dissipation: 520 mW @ 80 MHz (Core and I/O powered at 3.3V).

3.4. Antenna

[53] The SHARAD antenna is a 10-m dipole made of two 5-m foldable tubes, which, in stowed configuration, are kept in place by a system of cradles and, when released, will self-deploy because of their elastic properties. Electrically, the antenna is fed at the center, interfacing with the SEB by means of two wires (one for each dipole). The connected wires together form a balanced connection line. The line itself has no controlled impedance, and the load seen on the TFE side is therefore frequency dependent, requiring frequency compensation within the TFE.

[54] The antenna also includes its release mechanism (two solenoid controlled actuators to release the right and left dipoles). During deployment operations, heaters installed on the spacecraft panel will heat the antenna cradle hinges in order to keep the actuator mechanism within a suitable temperature range. A picture of the SHARAD antenna during a deployment test is shown in Figure 6.

4. SHARAD Performance

4.1. Link Analysis, Doppler Focusing, and Resolution

[55] The SHARAD instrument is designed to radiate 10 Watts to achieve a specular surface Signal-to-(Galactic)-Noise Ratio (SNR) of 50.6 ± 1.25 dB. The SNR depends on a number of factors and can be expressed as

$$SNR = \frac{P_p G^2 \lambda^2 \Gamma}{64\pi^2 R_0^2 K T_g B_N L}, \quad (2)$$

where P_p is transmitted power, G is antenna gain, λ is wavelength, Γ is surface power reflection coefficient, R_0 is distance from spacecraft to surface, T_g is the limiting galactic noise temperature, K is Boltzmann's constant, B_N is bandwidth, and L is propagation loss.

[56] Table 3 shows the SNR at the point of Analog-to-Digital Conversion (ADC) using the uncertainty only in the parameters that are not surface model dependent. Additional signal power is subsequently obtained by range (G_r) and Doppler (G_a) focusing or gain. The range compression gain is the time-bandwidth product ($B\tau$) of the 10-MHz bandwidth/85 μsec chirp signal, $B\tau = 10{\cdot}10^6$ Hz $\times$ $85{\cdot}10^{-6}$ sec = 850 (29.3 dB). Because the chirp signal is weighted (done in ground processing, nominally using a Hanning function) to reduce range sidelobes, the pulse compression is not ideal and loses up to 1.8 dB in gain. The actual compression gain in range, G_r, is then taken as 27.5 dB.

Table 3. Link Analysis for SHARAD

Parameter and Units	Nominal Value (Linear)	Uncertainty (Linear)	Requirement (Linear)	Contribution to SNR, dB	Margin, dB
		Signal Contribution			
Peak power	10 W	± 2.5 W	>10 W	10	−1.25[a]
Antenna gain	1			0	
Wavelength	15 m	negligible	15 m	23.5	
Surface Fresnel reflectivity	0.1	model dep.		−10	
$64\pi^2$	631.7			−28	
Range	320 km[b]			−110	
Receiver gain max				87	
Losses	3.2		N/A	−5	
Signal power at ADC				−2.5 dBm[c]	
		Noise Contribution			
Boltzmann constant	1.38×10^{-23} J/K			−228.6	
Galactic noise temp., T_g	$10^{4.9}$ K			49	
Noise bandwidth (MHz)	10	negligible		70	
Receiver gain max				87	
Losses	3.2			−5	
Noise power at ADC				2.4 dBm	
SNR at ADC				−4.9 dB	−1.25

[a]Worst case.
[b]Worst case in Primary Science Phase (PSP) of mission.
[c]Power of signal in dB referenced to one milliwatt.

[57] The azimuth (along-track or Doppler) gain is assumed, conservatively, to be no larger than the coherent integration of signals returned from the first Fresnel zone. The spacecraft-to-surface distance, R_0, can vary between approximately 255 and 320 km over an MRO orbit. This leads to a Fresnel zone diameter range of

$$D_{FZ} = 2 \cdot \sqrt{\frac{\lambda R_0}{2}} = 2765\,\mathrm{m} \rightarrow 3098\,\mathrm{m}. \tag{3}$$

The azimuth gain is given by

$$G_a = \frac{\frac{L_{syn}}{V_{S/C}}}{\frac{1}{\mathrm{PRF}}} = \frac{\frac{2765\,\mathrm{m} \rightarrow 3098\,\mathrm{m}}{3400\,\mathrm{m/s}}}{\frac{1}{700\,\mathrm{Hz}}} = 563 \rightarrow 633 \approx 28\,\mathrm{dB}\,, \tag{4}$$

where $V_{S/C}$ is spacecraft horizontal velocity and L_{syn} is the synthetic aperture length, taken as the diameter of the Fresnel zone. Note that 1/PRF is the pulse repetition interval, PRI, in seconds, so

$$G_a = \frac{L_{syn}}{V_{S/C}\mathrm{PRI}} = \frac{L_{syn}}{L_p}\,, \tag{5}$$

where L_p is the distance traveled by the spacecraft between pulses. Thus G_a can be interpreted simply as the number of pulses available for integration within a Fresnel zone. The realization of G_a is based on the premise that coherent integration can be performed for returned pulses from a ground patch of Fresnel-zone size.

[58] The focused signal-to-noise ratio, SNR_f, is then logarithmically the sum:

$$\begin{aligned}\mathrm{SNR}_f &= \mathrm{SNR} + G_r + G_a \\ &= -4.9 \pm 1.25 + 27.5 + 28 = 50.6 \pm 1.25\,\mathrm{dB}.\end{aligned} \tag{6}$$

The dynamic range for a subsurface-signal-to-noise ratio of 3 dB is then 47.6 ± 1.25 dB. The penetration depth (maximum depth for a 3-dB detection of a subsurface reflector) for the radar depends on (1) the path loss, a function of f, and integrated values of $\tan\delta$ and ε_r; (2) the reflection loss at the subsurface reflector; (3) the transmission losses at shallower dielectric interfaces in the signal path, and (4) the volume scattering loss. The last two losses are not accounted for in equation (1). For the very simple model of a dielectric interface separating a dry, porous (30%) material above and the same material with ice-filled pore spaces below, the penetration depth ranges from 200 m to 1500 m for a $\tan\delta$ and ε_r range from 0.03 and 9 to 0.004 and 5, respectively.

[59] Without Doppler focusing, the horizontal ground resolution can be taken as ranging from the diameter of a Fresnel zone (∼3 km) to the pulse-limited diameter [$2\sqrt{(C_0 R_0/B)}$, C_0 = free-space velocity], about twice this value. The Fresnel-zone resolution will be realized for relatively smooth surfaces. For more typical surfaces, the pulse-limited diameter is more realistic. This is the cross-track resolution range for SHARAD given in Table 2.

[60] Synthetic aperture focusing can improve the along-track (azimuth) resolution without sacrificing the SNR. The azimuth spatial resolution, ρ_a, is given by approximately (300-km spacecraft altitude)

$$\rho_a \approx \frac{\lambda R_0}{2D_{FZ}} = 750\,\mathrm{m}, \tag{7}$$

where for simplicity we have ignored the small difference between spacecraft and ground velocities. The azimuth resolution improvement C_a, is given approximately by

$$C_a \approx \frac{2D_{FZ}^2}{\lambda R_0} = 4, \tag{8}$$

which is of course the ratio of the Fresnel zone diameter to the azimuth spatial resolution.

[61] The azimuth signal is highly over-sampled by the 700 Hz PRF. As long as the spatial extent of the pulses involved in onboard coherent summing does not exceed the azimuth resolution, then there is no resolution degradation. The number of pulses that could be summed in 750 m is

$$\#\ \text{pulses summed} \approx \frac{\rho_a}{V_{S/C}}\text{PRF} = \frac{750\,\text{m}}{3400\,\text{m/s}}700\,\text{Hz} \approx 150\ \text{pulses}. \quad (9)$$

The actual onboard presumming range is 1 to 32 samples (pulses), so this implies that even with the maximum amount of onboard presumming, additional coherent summing will have to be done on the ground to achieve the full SNR. The azimuth focusing process will, by design, integrate pulses that are over-sampled along the ground track for the realizable Doppler spectrum. Note that before presumming on board, phase compensation with respect to the 20 MHz center frequency can be carried out to compensate estimated phase changes in the reflected signal due to the spacecraft radial velocity component and the surface slope. Information about these two quantities for specific data takes is uploaded to the spacecraft in the form of polynomial coefficients. The utility of the slope correction needs to be evaluated, since it carries uncertainties related to the spacecraft position predictions and surface topography, and it makes assumptions about the scattering properties of possible subsurface interfaces.

[62] It is of course possible to construct longer synthetic aperture lengths, and thus obtain finer azimuth resolution, for rougher surfaces that provide backscatter beyond a Fresnel zone distance of spacecraft motion. This could reduce surface clutter, particularly from compact scatterers. If a subsurface reflector is relatively smooth in this case, then the improved azimuth resolution would not be realized for the subsurface feature, but the ratio of power from subsurface reflections to surface scatterers should increase. The SHARAD azimuth (along-track) resolution given in Table 2 reflects a range about the nominal value of 750 m derived from the Fresnel zone synthetic aperture length (equation (7)).

4.2. Prelaunch Performance

[63] The performance of the radar was measured during the final tests before launch. The key radar performance parameters are radiated power, range resolution, and range sidelobe characteristics. The radiated power was measured to be slightly greater than 10 W, which is consistent with the link budget presented above. The measured instrument range resolution defined at 4 dB points is 15 meters in free space and 24 meters if a Hanning window is used for range sidelobe suppression. Sidelobe levels with Hanning weighting were well below those specified by the science requirements (see Figure 9).

4.3. EMI

[64] Electromagnetic interference (EMI) from the SHARAD radar itself, the S/C and other instruments degrade the signal-to-noise ratio of SHARAD. In an extreme case, these unwanted electromagnetic signals can saturate the receiver and render the instrument useless. As a result, special care was taken to assure that the level of EMI is well below the saturation level. The ground tests originally showed EMI at levels that could have reduced the instrument dynamic range. After proper shielding of S/C cables, the level of EMI was reduced to an acceptable level. Further tests during the cruise phase with the stowed antenna demonstrated even lower EMI levels by about 4 dB, mainly due to the absence of the Earth background EMI signals. Even at the highest instrument gain setting, saturation occurs at a rate less than 5% of the time within the receive window, which has minimal impact on the signal quality. The current results may change slightly after the antenna is fully deployed. Since in general the EMI is not coherent with the instrument, the signal averaging will reduce the EMI, and as a result the degradation of the SNR is less than a few dB.

5. Instrument Calibration

[65] Two requirements for SHARAD instrument calibration are meaningful: the relative and absolute calibration. The relative calibration goal for SHARAD is derived from the primary science objectives. For example, mapping the distribution of water/brine and ice requires comparison of data collected at widely different locations on the Mars surface, and thus a degree of stability in the power reflection coefficient of the processed radar data is required. Given a hypothetical layer of brine at some fixed depth, we should be able to correlate observations of the interface at a range of observing latitudes. If all other factors (attenuation, surface roughness, etc.) were constant, we would wish to characterize the effective reflection coefficient of this interface to within about 30%. This corresponds to a relative calibration accuracy of $\sim$2 dB.

[66] For the absolute calibration of subsurface reflections, there is no requirement for SHARAD due to the model-dependent estimates of surface reflectivity, attenuation in subsurface layers, etc. However, calibration of absolute power returned from the surface is possible, if the transmitted power is well-calibrated, by effectively inverting the radar equation for the scattering cross section of the surface. Further assumptions are necessary of course to obtain a Fresnel reflection coefficient, but these can be minimized over a flat, smooth surface. A reasonable target for the absolute calibration is $\pm$2.5 dB, assumed to be a good trade-off between scientific requirements and feasibility.

[67] In order to obtain the desired accuracy, calibration of the instrument was performed on the ground and will be performed again in flight during the transition and operations phases.

5.1. Preflight Calibration

[68] The ground calibration checked the transmitter and receiver chain parameters, the reference oscillator parameters, the antenna radiation pattern (characterization only with mock-up and by simulation), and the end-to-end parameters. Given the antenna dimension and because the antenna behavior is strongly related to the position of the MRO solar arrays and the high gain antenna (HGA), its calibration will be performed in flight.

5.2. Transition Orbit Calibrations

[69] The main purposes of the MRO Transition Phase are to safely establish the Primary Science Orbit prior to solar

conjunction, to prepare the spacecraft for solar conjunction, and to reconfigure the spacecraft for science operations. Among the activities to be performed during the Transition Phase are the antenna deployment and SHARAD check-out, the SHARAD functional tests, and the SHARAD antenna calibration. The antenna deployment and SHARAD check-out included the following steps:

[70] 1. Antenna deployment verification: This was in fact achieved on 16 September 2006, in part, by performing several ''sniffs'' (SHARAD turned on in receive-only mode) before and after the antenna deployment, comparing the level of galactic noise received by the antenna. The expected increase in noise level due to the deployed antenna was observed.

[71] 2. Receiver check, galactic noise and EMI characterization: The same sniffs used for the confirmation of the antenna deployment were used to characterize the spacecraft electromagnetic environment and verification of interference line removal.

[72] 3. Transmitter check: The status of the transmitter was checked after deployment and was found to be operating within the expected range.

[73] 4. Surface echo check: The position of the range window was checked and the first echoes from the surface and subsurface were obtained on 18–19 September 2006.

[74] The SHARAD functional tests consist of transmitter/receiver-chain tests to ensure that Mars surface echoes are collected with different instrument configurations. These tests include data takes performed with different radar parameters, such as PRF, presumming, number of bits, dynamic and static scaling, and phase compensation. In addition, open-loop tracking mode and closed loop tracking mode tests will be performed to verify for both modes the end-to-end capability to correctly program the SHARAD range window position to follow the surface topography. ''Open-loop'' refers to preprogrammed information that sets the range window, while ''closed loop'' indicates that the range window is set by feedback from tracking the actual surface.

[75] The SHARAD antenna calibration is performed in passive radiometric calibration (aimed at characterizing the instrument in a receive-only configuration) and in active radiometric calibration (aimed at measuring the two-way pattern). The activities in this phase consist of a calibration for an arbitrary reference spacecraft condition, and then an antenna radiation pattern calibration for various spacecraft high-gain antenna and solar panel positions. This is done with the assumption (to be confirmed) that the spacecraft configuration does not affect significantly the shape of the antenna pattern, at least in the narrow sector of interest ($\pm 10^\circ$ pitch and $\pm 20^\circ$ roll with reference to nadir), but only its absolute amplitude. The antenna radiation pattern calibration will be performed, at least, for the combinations of the following pitch/roll values:

[76] 1. Pitch: -10°, 0°, $+10^\circ$.

[77] 2. Roll: -20° to $+20^\circ$ with 5° steps.

[78] The best approach to calibration is to take advantage of the orbit revisiting the same locales. Opportunities for revisit occur 12-13 times per day in both the northern and southern hemispheres, about 12 hours apart at the intersecting point of ascending and descending nodes. The goal is to minimize the scene dependence of the calibration.

[79] The antenna gain calibration will be performed with different S/C configurations, with nadir pointing only. The crossovers in the relatively smooth northern polar regions are the most attractive. On each crossover, an acquisition in the ''reference'' configuration and another in one of eleven other configurations (variability of solar arrays and HGA) is needed.

5.3. Primary Science Orbit Calibrations

[80] Activities during the transition orbits will not fully characterize all of the possible configurations for SHARAD calibration. Given that there are difficulties in fully characterizing the antenna pattern due to the varying backscattering properties of the surface and that only a limited number of orbits can be devoted solely to this task during the science data collection phase (nadir pointing), many orbits can be utilized for both scientific data analysis and simultaneous instrument calibration. In this way, many surface characteristics (flat and rough) can be analyzed during the normal scientific operations in order to permit averaging of the values to give a best estimate of antenna behavior.

6. Science and Sequence Planning

6.1. Overall Strategy

[81] By design, SHARAD is able to operate at any time while the MRO spacecraft is orbiting Mars, regardless of solar illumination conditions. Constraints on the actual operation of SHARAD during the mission come as a result of tradeoffs among the various instruments on board, which must share data volume as well as the spacecraft's pointing capabilities. SHARAD is fundamentally a nadir instrument, but it can still acquire good data in an off-nadir pointing attitude up to ten degrees. When MRO is pointed more than ten degrees off nadir to accommodate observation requests from the other instruments, SHARAD will not acquire data.

[82] During the night SHARAD will have first priority among MRO instruments. In fact, these nighttime observations by SHARAD are considered as ''Non Interactive Observations'' (NIO) because they do not impact the operations of the spacecraft or any other instrument. SHARAD will also take daylight observations of both Martian poles as part of its integrated polar campaign. During the Primary Science Phase (PSP), SHARAD will be allocated two hundred dedicated passes per pole (see section 9.2).

[83] SHARAD is essentially a survey instrument, building up meaningful data sets by multiple observations of a given area of interest. As a result, the vast majority of SHARAD observations will be planned with respect to target regions extending over tens or even hundreds of kilometers, an observational strategy that is distinctly different from the specific point targeting of the imaging instruments. Throughout the mission, to aid in the biweekly planning process, the SHARAD team will update a database including both the list of all desired targets of observation and maps of the acquired coverage.

[84] Another major part of the SHARAD operational planning is the determination of the settings for the key onboard parameters for each observational suite. Specifically, SHARAD has considerable freedom in both its preprocessing parameters and its data production rate, and

Table 4. Science Data Production Rate, Mbps, as a Function of Number of Pulses Presummed and Digitization Word Size

Presummed Pulses	4 bit	6 bit	8 bit
1	10.08	15.12	20.16
2	5.04	7.56	10.08
4	2.52	3.78	5.04
8	1.26	1.89	2.52
16	0.63	0.95	1.26
28	0.36	0.54	0.72
32	0.32	0.47	0.63

the early observations will be used to establish the optimal operating zone for the instrument. The data production rate for SHARAD, for example, can vary from as low as 300 kbps to over 20 Mbps, depending on the pulse repetition frequency, presumming strategy, and number of bits per sample. As the data volume for SHARAD is limited by the MRO allocation of 15% of its total data, which will typically range from 40 to 90 Gb/day, the number of observations that SHARAD can acquire in any given period is extremely dependent on the selected data production rates.

[85] The relationships among data production rate, presumming strategy, and bits per sample for SHARAD observations are shown in Table 4. The optimal choices for these parameters are in turn dependent on a broad variety of encountered conditions, ranging from the performance of the radar itself to the off-nadir clutter power to the surface roughness. Early in the mission, it is expected that different combinations of these parameters will be used to characterize SHARAD and estimate the impact of the Martian environment on the received signal.

[86] SHARAD will operate nominally in the open-loop tracking mode, at least during the early phase of its operation, and switch operation modes (e.g., presumming) according to a predetermined command sequence. Within any single orbit, the instrument can be operated (1) either continuously or discontinuously, (2) in any of its observation modes, and (3) in any desired sequence. This is true provided, as mentioned earlier, that for each biweekly observational period, the overall SHARAD data volume does not exceed 15% of the total MRO science data downlink. The anticipated data return for two years for all instruments is 34–50 Tb.

6.2. Science Planning and Target Database

[87] SHARAD targets (Regions of Interest, ROI) are specified in a target database by a polygonal area for coverage, and a science priority for this coverage. Planning tools query the database and match upcoming orbital data takes to the target database to generate a Payload Target File (PTF). Conflicts are resolved by target priority, and by human intervention as necessary. If no targets are available in an upcoming data take, then data acquisition is used to help fill in a global $5^\circ \times 5^\circ$ resolution exploratory grid.

6.3. Observation Sequence Planning

[88] Generally, SHARAD observations will be noninteractive (NIO) and therefore scheduled, according to the MRO operations strategy, on a weekly basis. However, when SHARAD is taking daytime measurements as part of its polar campaign, then its exact observation schedule must be negotiated with the other instruments at the biweekly Target Acquisition Group (TAG) meeting.

[89] Because of the stringent targeting requirements of the MRO science instruments, frequent orbit ephemeris updates must be calculated on the ground and uplinked to the spacecraft. As a result, the operational timeline does not always allow sufficient time for interaction with the SHARAD science team for detailed specification for each set of observations. However, the SHARAD Targets Database was designed to be automatically managed by the planning tool and to contain all the science team information that is needed to classify, every week, the set of all the observation opportunities. In addition, all possible targets are listed in the SHARAD Targets Database, along with their comparative scientific and operational priorities and their seasonal requirements. This target listing essentially provides guidelines to the SHARAD operations team in the selection of target sites.

[90] The output of the science planning phase, described above, will be the PTF. The PTF lists all scheduled observations in terms of orbit number, center latitude, and observation duration. In addition, the PTF includes all information required by the MRO planning team to determine the overall schedule and to merge the observations from the different payload elements, as well as the variables necessary for the spacecraft to generate the specific SHARAD commands. During the implementation of the observation sequence, these SHARAD commands will be generated by the spacecraft onboard software using both the target block and the variables contained in the ITL (Integrated Target List, which is the result of the integration of the PTF and subsequent conversion into the spacecraft format).

[91] To actually execute the SHARAD observations, the three binary files for each active orbital pass that need to be uplinked are the Orbital Data Table (ODT), Parameter Table (PT), and Observation Sequence Table (OST). The OST and PT files will be generated by the SHARAD operations team twice per week and submitted for uplink as a Non Interactive File Load (NIFL). The Orbital Data Table is subject to variations as a result of the spacecraft ephemeris updates. Therefore the actual SHARAD ODT files that are used on board will be generated and uplinked by the FET (Flight Engineering Team) after each ephemeris update.

7. Ground Data System (GDS) Design and Data Products

7.1. Downlink Processes

[92] The raw science data produced by SHARAD will be typical coherent radar data, i.e., samples of signal voltage and phase versus time of the received radar signals with a simple coherent presumming performed on board. During its operation SHARAD also produces housekeeping telemetry (engineering parameters, command acknowledgments, events, etc.) to enable ground monitoring of instrument operations.

[93] When SHARAD is operating, SHARAD engineering telemetry packets are interleaved with the science telemetry packets on the portion of the MRO Solid State Recorder (SSR) that is set aside for SHARAD. The MRO flight software subsequently packetizes all the SHARAD data,

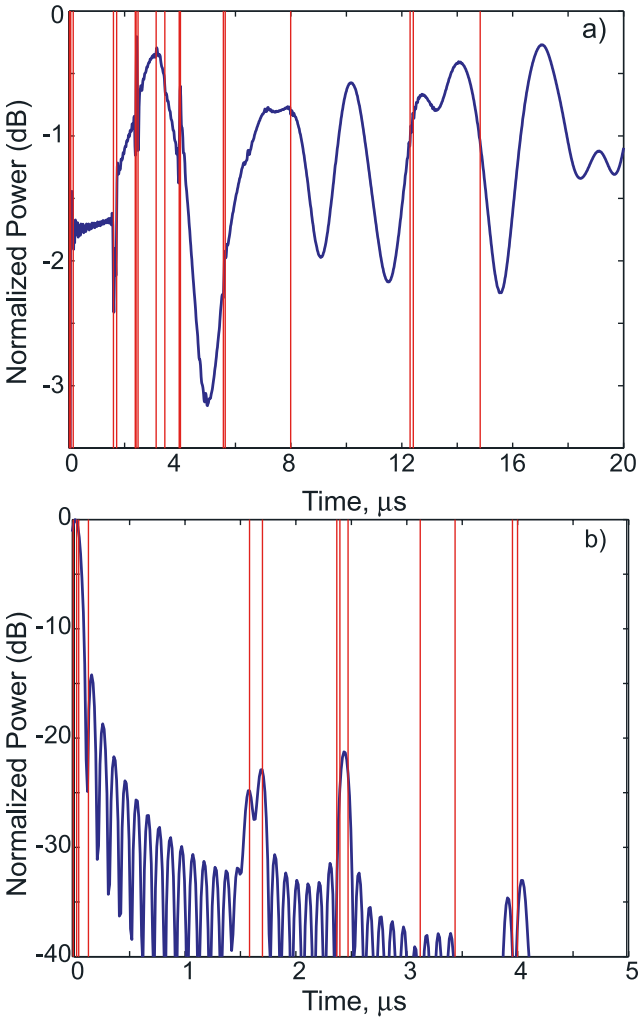

Figure 7. (a) Simulation of SHARAD EDR data from a plane parallel Martian stratigraphy (as described by *Shchuko et al.* [2003]). Plot represents the power received by the instrument as a function of time. The vertical lines mark instants of time in which an echo from a subsurface dielectric interface reaches the radar. (b) Simulation of SHARAD RDR data from a plane parallel Martian stratigraphy (as described by *Shchuko et al.* [2003]). Plot represents the power received by the instrument as a function of time after range compression. The vertical lines mark instants of time in which an echo from a subsurface dielectric interface reaches the radar. Peaks corresponding to individual subsurface reflections are clearly visible. Echoes coming from layers that are too deep or too close to each other are not discernible. Note also the sidelobes associated with each of the echoes. No weighting has been applied to reduce sidelobes (see section 9.4).

according to a predetermined scheme, and sends it to the ground via the downlink. The SHARAD products received on the ground will thus be a mix of science and instrument engineering health data, along with housekeeping data associated with telemetry products. The MRO ground data system eventually places these SHARAD data on the Raw Science Data Server (RSDS), where it is available to the SHARAD operations team.

[94] In the SHARAD Operations Center, SHARAD data processing will be performed daily, from Monday to Friday. This processing is accomplished by software that falls into three general categories: instrument monitoring, quick look assessment, and science processing. The instrument monitoring software performs packet deformatting, instrument health assessments, and instrument sequence verification. The quick look software provides a rapid assessment of the scientific performance of the SHARAD instrument. The science processing software, as its name suggests, encompasses the full range of raw SHARAD and ancillary data processing necessary to understand the SHARAD data, including interleaving Doppler and range information plus the reconstructed ground tracks, and using Mars Orbiter Laser Altimeter (MOLA) topography data for the identification of possible clutter features.

[95] The data volume from SHARAD will be large (15% of 34–50 Tb), exceeding both the entire Magellan data volume and twice the data volume of the primary Cassini mission (all instruments).

7.2. Data Processing and Standard Data Products

[96] All data released by the SHARAD Team for archiving are required to be compliant with the Planetary Data System (PDS) standard [*PDS*, 2003]. This standard imposes requirements on several aspects of the data product generation process, among which is a need for detailed documentation describing the origin, structure and processing undergone by data, for their accurate location in space and time, and in general for all auxiliary and ancillary data that are needed for the scientific use of the data product.

[97] The SHARAD team plans to produce and distribute two sets of standard data products, called Experiment Data Records (EDRs) and Reduced Data Records (RDRs).

[98] Experiment Data Records: The EDRs will consist of the instrument scientific telemetry correlated with the auxiliary information needed to locate observations and to process data further. EDR data users will mainly be radar scientists interested in doing the entire processing of the received signal. The fact that unprocessed echoes do not show any obvious indication of subsurface interfaces will make EDRs of little use to the planetary geoscience community in general (Figure 7a).

[99] Each EDR "Data Product" is an aggregation of SHARAD data blocks. A data block is produced through the onboard processing of one or more received echoes, and constitutes a single observation of the instrument. Each Data Product will contain data from one or more data blocks collected continuously using the same operation mode, instrument status and onboard processing scheme. The content of each EDR Data Product is highly variable in terms of number of data blocks, and depends on how operations for the instrument were planned during a given data collection period.

[100] Reduced Data Records: SHARAD achieves its spatial resolution, both in depth (or range) and along the ground track, only after processing of the received echo on the ground. The method through which vertical resolution is achieved is called range processing, or range compression, while horizontal resolution is enhanced through what is

called azimuth, Doppler, or synthetic aperture processing (see section 4.1).

[101] Reduced Data Records will consist of received echoes that have been Doppler focused, range compressed and converted to complex voltages, and correlated with the auxiliary information needed to locate observations in space and time and to process data further. RDR users are expected to be mainly planetary geoscientists interested in determining the structure of the shallow Martian subsurface (see Figure 7b). Data users must be aware that processed echoes may contain artifacts due to off-nadir surface reflections, or clutter, reaching the radar after nadir surface echoes, and thus possibly appearing to be subsurface reflections (see section 8).

[102] Each SHARAD RDR Data Product is the result of the processing of all echoes acquired continuously in time using the same operation mode, instrument status, and onboard processing scheme. There is one RDR Data Product for every EDR Data Product acquired in subsurface sounding mode, the latter in fact constituting the sole input for the RDR product generation. The content of each SHARAD RDR Data Product is highly variable in terms of number of processed echoes, and depends on how operations for the instrument were planned during a given data collection period.

7.3. Public and Project Access to SHARAD Data Products

[103] EDR Data Products, Experiment Status Report Files and calibration files are produced at the SHARAD Operations Center located in Rome, Italy. The production of RDRs will also take place at the SHARAD Operations Center, using the EDR data archive as its sole input. The rate of RDR data production will keep pace with EDR data production, although there could be some delay (on the order of a few days) due to the need to verify the content and quality of EDR Data Products used as input.

[104] After a data validation period of 6 months or less, the SHARAD team will notify the PDS that certain products have been validated and are ready to be made available to the broader planetary community.

[105] The PDS will distribute SHARAD data through its Geosciences Node. Data will be available on-line through a set of PDS search and retrieval tools that will provide access to data from all Mars missions. The user will be able to search for and retrieve data that meet criteria such as a specific time interval, instrument, or location on the planet. Map-based searches will also be supported as appropriate. Data will be made available via electronic transfer and as custom volumes generated on digital media.

8. Surface Clutter Mitigation

[106] The goal of a radar sounder is to identify echoes from subsurface dielectric discontinuities that may be linked with geological features such as layering, fault/impact structures, or compositional changes. Doppler (synthetic aperture) processing is used to narrow the effective along-track region from which echoes may be received, but there is little that can be done to reduce the large physical area of the surface illuminated in the cross-track (range) direction. This allows reflections from surface topographic features, including those well away from the nadir track, to arrive simultaneously with echoes from subsurface reflectors directly beneath the sounder [e.g., *Phillips*, 1973]. The resulting ambiguous surface contributions are termed ''clutter.'' Clutter can arise from two general types of topography. ''Statistical'' clutter refers to the time-broadening of the near-nadir radar echo from the surface due to random roughness at spatial scales comparable to or greater than the illuminating wavelength. ''Deterministic'' clutter refers to echoes from discrete surface features, such as hills or crater walls, which may be many times the illuminating wavelength in size.

[107] Statistical clutter, often described by a quasi-specular scattering law such as that proposed by *Hagfors* [1964], cannot be readily suppressed, and thus tends to set the ''signal-to-clutter'' ratio for sounder performance. In practice, a rougher surface (on scales of the illuminating wavelength and larger) will have a broader distribution of echo power with time delay, and this will tend to mask reflections from the shallow subsurface. Smoother terrain is thus more amenable to sounding. Analysis of the dominant scattering regime for slightly rough surfaces shows that the statistical clutter may exhibit rapid variations in brightness as the terrain shifts from coherent to incoherent scattering modes [*Campbell and Shepard*, 2003].

[108] Deterministic clutter is more problematic, because extended surface features such as ridges can mimic strong subsurface reflecting horizons. One goal of sounder data analysis is thus to identify echoes from the surface, and to suppress these with as little impact as possible on the ''true'' subsurface reflections. There are several means for achieving these goals. The most robust method, in a technical sense, is to use closely-repeated sounder orbital passes to permit interferometric correlation. The echoes from a surface feature will appear at different effective ranges in the two passes, while those from a horizontal subsurface layer will be at a similar range. The correlation of the two data sets will thus tend to coherently enhance the signal from subsurface horizons and reduce those of surface clutter. The SHARAD system does not permit very stable time-base measurements required for inter-orbit phase stability, so we do not expect that this technique can be employed, except on an experimental basis for areas where we can establish the relative phase from the surface echo. However, techniques using only signal power to search for features with stereo separation between radar returns acquired on parallel orbit tracks [*Phillips et al.*, 1973] can separate surface scatterers from horizontal subsurface layers. This technique was used successfully [*Peeples et al.*, 1978] to map subsurface reflectors in Mare Serenitatis and Mare Crisium with the Apollo Lunar Sounder Experiment (Figure 2).

[109] A second method, now widely used for MARSIS data analysis, employs the MOLA digital elevation model (DEM) to predict the quasi-specular scattering behavior of the surface topography for any given ground track [*Picardi et al.*, 2005]. The resulting ''synthetic'' echo profiles are used to identify reflections that clearly do not arise from the subsurface. Figure 8 shows the MARSIS radargram from Mars Express Orbit 2737, along with the model radar response from surface topography. The model provides a good match to the radar data, providing an immediate classification of surface signals that might be mistaken for

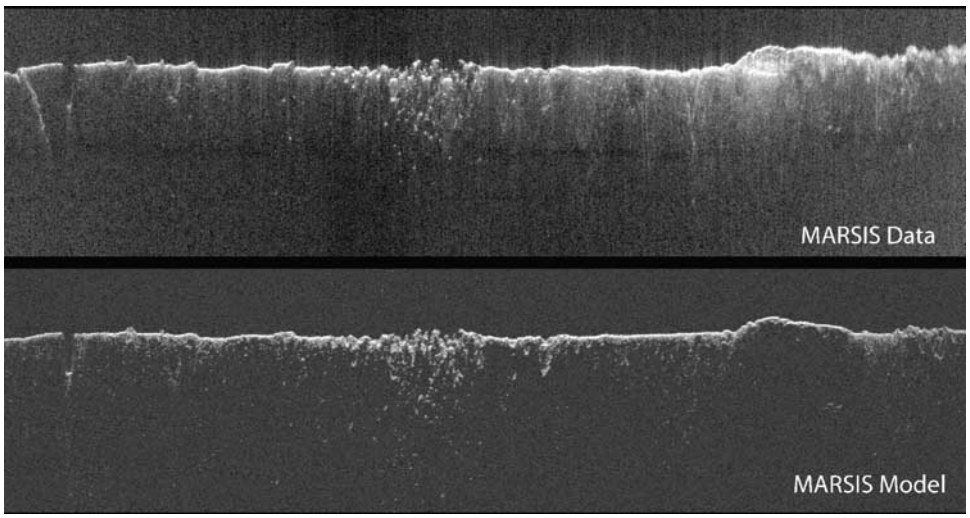

Figure 8. (bottom) MARSIS clutter simulation model using MOLA DEM for Mars Express Orbit 2737. (top) MARSIS radargram for same orbit. Note features near relatively steep slope on right that do not show up in the simulation.

subsurface features, and, conversely, indicating features in the data that have no counterpart in the predicted scattering. Radar simulations of surface topography may not be as effective for SHARAD; the shorter wavelength of this radar pushes the resolution available in the MOLA DEM. Nevertheless, early modeling results employing the SHARAD signal have been encouraging. A complementary method projects time delay data in the range direction to the cross-track location on the surface with the same time delay [*Holt et al.*, 2006b; *Picardi et al.*, 2005; *Watters et al.*, 2006]. This facilitates identification of surface features, though there is a left-right ambiguity in the projections due to the nature of the dipole antenna pattern.

[110] Finally, we are considering approaches that exploit the full synthetic aperture operation of SHARAD to discriminate surface from subsurface features. For example, the echoes from surface topographic features may have more extended Doppler signatures (i.e., appearing further behind and ahead of the nadir point) than subsurface reflections, which largely depend upon coherent reflection from favorably oriented (near-horizontal) parts of a dielectric horizon.

[111] The radargrams may also suffer from ''speckle noise,'' resulting from random constructive and destructive interference from individual scatterers within a resolution element. Standard data products will not address speckle (e.g., using ''multilooks''), but end users can reduce speckle in the RDRs by spatial averaging.

9. SHARAD Science Targets

[112] Below we discuss some specific SHARAD targets. This is not intended to be a complete list. We have left out, inter alia, peri-polar terrains, buried drainage networks, and volcanic features. There are in reality a vast number of subsurface targets for SHARAD, some based on knowledge of Mars geology, and others based on MARSIS results [*Picardi et al.*, 2005].

9.1. Polar Layered Deposits

[113] As mentioned in section 2, the MARSIS signal is able to penetrate the entire stack of polar layered deposits and to partially resolve internal layering (Figure 3). As also discussed earlier, the path loss of the MARSIS signal is extremely low, implying that SHARAD will also likely penetrate the stack, but with much better vertical resolution. Figure 9, adapted from *Nunes et al.* [2006], shows model results for both MARSIS and SHARAD radars for an assumed dielectric model obtained from (1) relating visible albedo variations from the Mars Orbiter Camera (MOC) to silicate fraction variations, (2) assuming the high and low albedo extremes correspond to silicate fractions of 1% and 10%, respectively, and (3) employing mixing models using standard dielectric constants for ice and silicates [*Nunes and Phillips*, 2006]. In these results, SHARAD does a better job of resolving individual layers, while strong MARSIS reflections, except at major boundaries, result from the integration of several unresolved reflectors. We note that the layering variability observed in MOC images is beyond even SHARAD resolution, though these fine-scale variations reflect relatively small changes in albedo [*Nunes and Phillips*, 2006, Figure 3].

9.2. SHARAD Polar Seasonality Campaigns

[114] Besides extensive spatial coverage of the polar regions, the SHARAD experiment will build up a time series ($\Delta Ls \approx 18^\circ$) by repeated sampling over $\sim$13 ground tracks equally spaced in longitude over both poles. The objectives are to (1) monitor the change in surface reflection coefficient as a function of season and locale and (2) examine the seasonal dependence of the exploration depth of the radar. The first objective explores the concept that SHARAD can be used to monitor the comings and goings of seasonal deposits [*Nunes and Phillips*, 2006]. To that end, there will be simultaneous observations by CRISM (Compact Reconnaissance Imaging Spectrometer

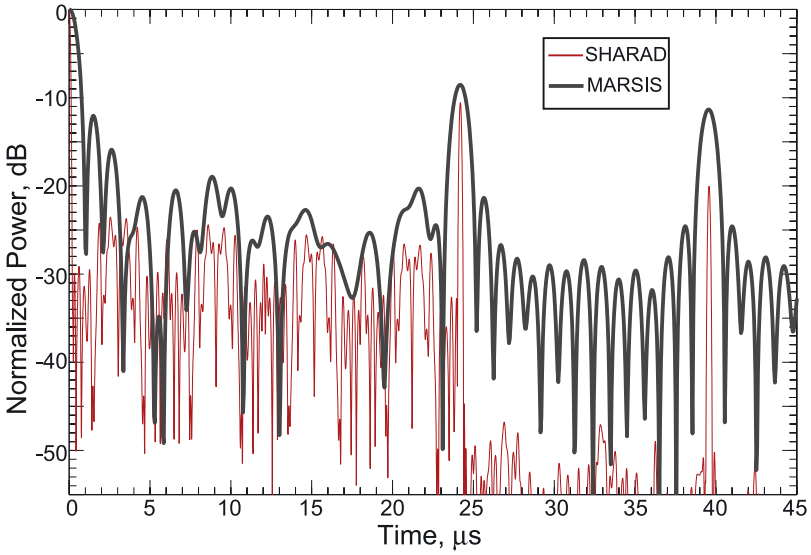

Figure 9. A comparison of MARSIS and SHARAD radar signal predictions over the North Polar Layered Deposits (NPLD) [*Nunes et al.*, 2006]. The NPLD can be divided into an upper and lower unit [*Byrne and Murray*, 2002; *Fishbaugh and Head*, 2005]. For the upper unit, albedos derived from 250 vertical meters of MOC data have been extended by cyclically repeating albedo over the whole unit. Albedo, in turn, is converted to silicate fraction in the polar layered deposits, but suffers from nonuniqueness due to unknown grain size. Here, minimum and maximum silicate fractions are assumed to be 1% and 10%, respectively, and other silicate fractions are scaled from albedo. The lower unit, likely a paleo-erg, is assumed to have a constant silicate fraction of 50%. Dielectric constant of composite ice/silicate material is obtained using an appropriate mixing formula with the dielectric constant of ice and silicate inclusion given by $\varepsilon_i = 3.15 + i6.30 \times 10^{-4}$ and $\varepsilon_s = 8.80 + i1.70 \times 10^{-2}$, respectively. The NPLD is assumed to be underlain by basaltic crust. Reflections from the UPLD/LPLD (2-km depth) and LPLD/basalt (3-km depth) interfaces arrive at 24 μs and 39.5 μs, respectively. The one-dimensional radar signal from this model is obtained using the approach of *Nunes and Phillips* [2006]. The stronger subsurface reflections can be confidently identified as those signals that stand above what is a rapid decay with time of the sidelobes (see Figure 10).

for Mars) in its hyperspectral central scan mode to examine variations in seasonal frost.

9.3. Buried Craters

[115] Mentioned briefly in section 2, a second class of apparent subsurface reflectors found by MARSIS is that of buried impact craters [*Picardi et al.*, 2005; *Watters et al.*, 2006]. These craters typically do not correspond to the nearly-buried craters (Quasi-Circular Depressions, QCDs) found by detailed analysis of MOLA data [*Frey et al.*, 2002]. The QCDs have been used to justify a much older age for the northern lowlands crust than that estimated from most earlier studies. If the MARSIS detections are real, then this lack of correlation is understandable if the MARSIS-found craters are buried to the extent that they do not have even a subtle surface topographic expression. More puzzling is the observation that the QCDs for the most part do not show up as nearly buried craters in the MARSIS data. Possibilities for this discrepancy are that there are valid but almost completely independent populations (MARSIS-found, MOLA-found) of buried craters, the QCDs are suspect, or only special circumstances allow a buried basin to be detected by MARSIS (e.g., sufficient dielectric contrast of fill with preexisting crater floor and wall). SHARAD may help resolve this controversy with higher resolution and more spatially extensive coverage of the northern lowlands.

9.4. Mapping Shallow Ice Depth

[116] The Neutron and Gamma-Ray Spectrometers on the Mars Odyssey spacecraft discovered abundant evidence for subsurface ice [e.g., *Boynton et al.*, 2002]. While the depths to the top of the ice (typically < 10 cm) are predicted by theoretical models [*Mellon and Jakosky*, 1995] that are in good agreement with the Neutron Spectrometer data set [*Mellon et al.*, 2004], depths to the bottom of the ice are poorly known. If the ice in the shallow subsurface is just that amount in equilibrium with the atmosphere, rather than the top of a deep reservoir, then the equilibrium depth to the bottom of the ice is estimated to be in the range of 10–20 m when the thermal conductivity of ice in the pore spaces is taken into account (M. Mellon, personal communication, 2005). Estimating, or at least constraining, the subsurface ice volume is extremely important in understanding the present-day global water inventory of Mars.

[117] Given SHARAD's vertical resolution, detecting dielectric interfaces in the 10–20 m depth range seems feasible. However, resolution close to the theoretical limit can only be achieved when resolving signals of equal strength, which is not the case when attempting to detect

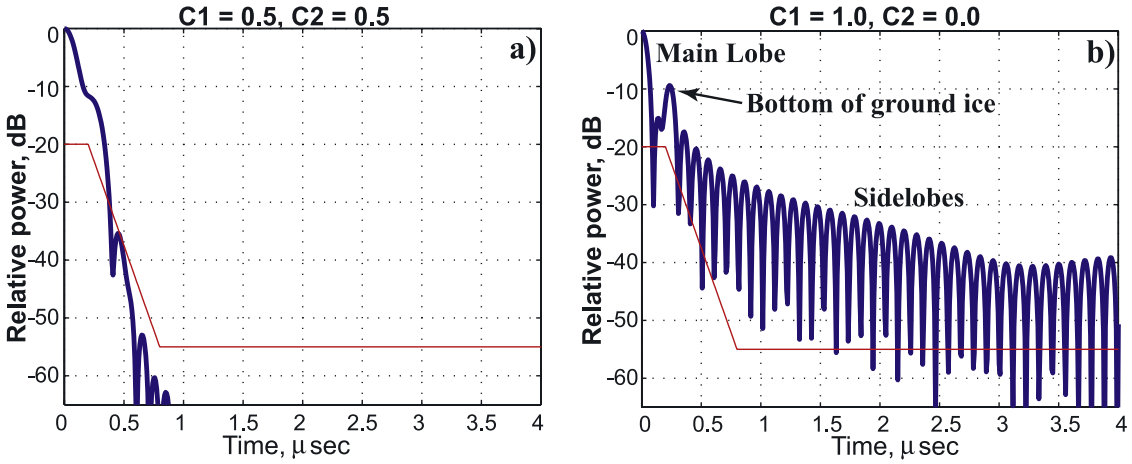

Figure 10. Model SHARAD detection of bottom of ice-filled pore space at 15 m depth. (a) Nominal SHARAD Hanning weighting. (b) No weighting at all. The red line gives the sidelobe specification for the SHARAD design, which has been achieved in the flight instrument with Hanning weighting.

a relatively weak signal from the base of the ice in the presence of a strong surface reflection. Any finite-bandwidth signal will have a power profile in the time domain of the form roughly $[\sin(at)/t]^2$, where a depends on bandwidth. Such a signal is described by a main lobe centered at $t = 0$, with sidelobes extending outward. A major issue for subsurface sounding is controlling the strength of signal sidelobes, so that weak subsurface returns are not swamped by the sidelobes of the stronger reflection from the surface. Sidelobes are typically muted by using a weighting function to taper the reconstructed radar signal used for pulse compression. One class of weighting functions is given by $w(t) = C_1 - C_2\cos(2\pi t/T)$ for pulse length T, where $C_1 + C_2 \equiv 1$. Nominal SHARAD data processing for best sidelobe control is achieved with a Hanning function ($C_1 = C_2 = 0.5$). Good sidelobe control is achieved, however, at the expense of widening the signal's main lobe. While this is generally not a problem, it hinders detection of shallow subsurface reflections, such as those expected from the bottom of atmosphere-equilibrated ice.

[118] Figure 10 shows the range-focused (chirp compressed) results for a shallow subsurface model with 10 cm of dry soil underlain by 15-m of ice-filled pore space (40% porosity). The main features of the modeled radar signal are the strong return of the surface echo and a weaker reflection from the bottom of the ice-saturated zone. Figure 10a shows that with Hanning weighting, the 15-m deep reflection is not resolvable from the main lobe of the surface reflection. Note that the theoretical resolution, based on bandwidth, is less than 10 m. Figure 10b shows that when weighting is turned off, the main lobe narrows, the sidelobes of the surface reflection are considerably larger, but the subsurface reflection is easily resolvable. The main point to be made here is that the choice of parameters in ground data processing matters, and one size does not fit all. Furthermore, a confident interpretation of a shallow reflection in terms of the dielectric interface at the bottom of the ice layer could depend on the correlation of the radar results with observables that might control the ice-bottom depth. These include latitude, albedo, thermal inertia, and local slope.

9.5. Mapping the Etched Terrain

[119] The MER rover Opportunity landed in a hematite-rich region in Terra Meridiani. Earlier geomorphic mapping showed that the hematite occurrence was part of an extensive stack of Noachian layered deposits [*Hynek et al.*, 2002]. An important multilayered member of this group, termed "etched terrain," is a differentially-eroded unit that is high in both thermal inertia and albedo [*Arvidson et al.*, 2003; *Hynek et al.*, 2002]. At the Opportunity landing site, hematite spherules weather out of a sulfur-rich bedrock [*Squyres et al.*, 2004] that is in fact within the layers of the etched terrain [*Hynek*, 2004]. Etched terrain is exposed over at least 3×10^5 km^2 in the Meridiani and western Arabia Terra regions [*Hynek*, 2004], yet is seen to disappear under younger units (Figure 11). As this sulfate-rich unit [*Gendrin et al.*, 2005], in places hundreds of meters thick, is likely indicative of the Noachian occurrence of water at or near the surface, mapping the extent of the etched terrain is fundamental to estimating the magnitude of Noachian surface water occurrence.

[120] SHARAD has an important role to play in the mapping of the sedimentary sequence in Terra Meridiani. As a guide to radar reflection properties, we note that the dielectric constant of anhydrite is about 6, so a reasonable dielectric contrast with other geological materials might be expected. Further, the large thermal inertia of the etched terrain implies that it is a relatively highly indurated geological material, implying further that it has a higher density, and hence higher dielectric constant, than interbedded low thermal inertia units. Note that the subsurface power reflection coefficient, R_{12}, at a planar interface between materials with dielectric constants ε_1 and ε_2 is given by $R_{12} = [(\sqrt{\varepsilon_1} - \sqrt{\varepsilon_2})/(\sqrt{\varepsilon_1} + \sqrt{\varepsilon_2})]^2$. Thus SHARAD has a reasonable probability of mapping subsurface layering within the etched terrain. Further, because this unit is exposed at the surface, it

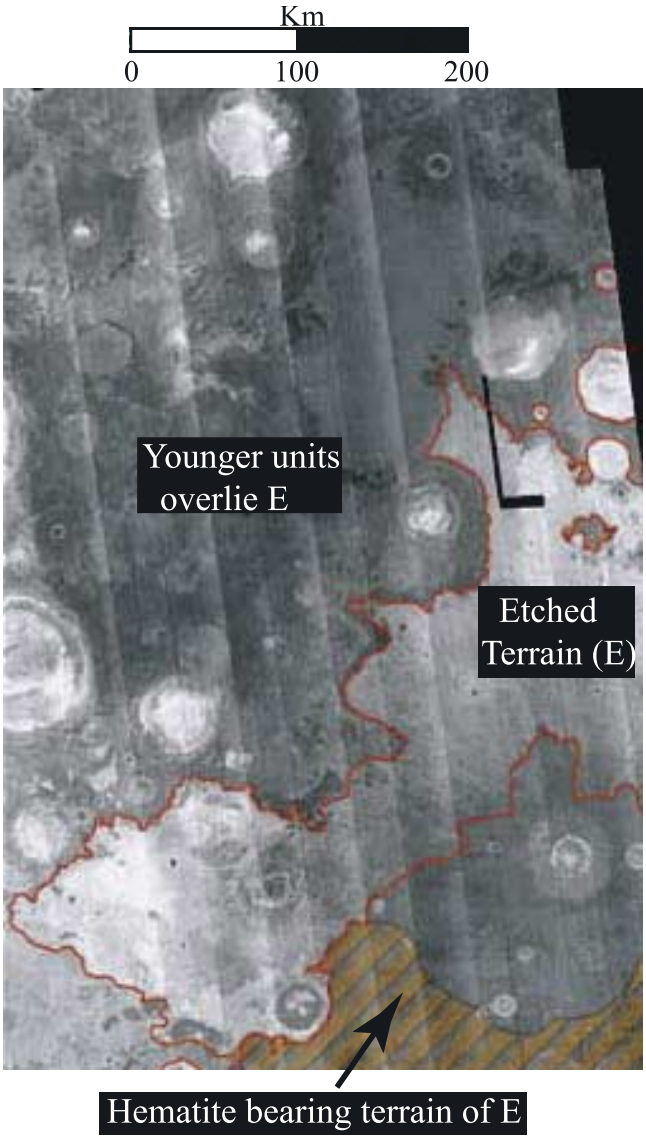

Figure 11. Thermal inertia map of a portion of the Terra Meridiani – W. Arabia Terra region of Mars derived from THEMIS data [*Putzig et al.*, 2004]. Thermal inertia increases from black to white in the image. Etched terrain (E) and hematite-bearing units are indicated. Etched terrain is buried to the north but is exposed in some craters. Adapted from *Hynek* [2004] with permission from Macmillan Publishers Ltd.

can be "followed" from there into the subsurface, giving confidence to its identification in SHARAD subsurface radar returns.

10. Concluding Remarks

[121] The SHARAD instrument will be the second sounding radar to operate in orbit around Mars. The MARSIS radar on Mars Express was designed for deep penetration with relatively coarse resolution, while the SHARAD radar should have relatively less penetration, but an order of magnitude improvement in vertical resolution and nearly that in horizontal resolution. In contrast to MARSIS, essentially all of the SHARAD data processing will be on the ground, which allows flexibility in processing parameters and optimization for specific targets.

[122] MARSIS has already been successful in penetrating both polar caps to the underlying basement, in mapping interfaces within the polar layered terrain, and in mapping buried craters in the northern lowlands. Orbital sounding radar works well at Mars. Because of its superior vertical resolution, SHARAD's forte may well be that of a stratigraphic mapper, revealing more detail in the polar layered deposits and adding the third dimension to our knowledge of the structure of sedimentary layers observed at many places on Mars.

[123] All indications are that the instrument will operate as designed, and EMI will have an insignificant effect on data quality. The biggest challenge to data interpretation will be from the interfering effects of surface clutter.

[124] **Acknowledgments.** This work was supported by the Italian Space Agency (ASI, Agenzia Spaziale Italiana) and by the NASA Mars Reconnaissance Orbiter project at the Jet Propulsion Laboratory (JPL), California Institute of Technology. We would like to thank Enrico Flamini of ASI, the SHARAD team at Alcatel Alenia Spazio in Rome (especially Enrico Zampolini), the MRO Project office at JPL (especially Jim Graf and Rich Zurek), and the engineering team at Lockheed Martin in Denver (especially Joe Witte). We also thank two anonymous reviewers for their thorough reviews, which greatly improved the clarity of the manuscript.

References

Arvidson, R. E., F. P. Seelos IV, K. S. Deal, W. C. Koeppen, N. O. Snider, J. M. Kieniewicz, B. M. Hynek, M. T. Mellon, and J. B. Garvin (2003), Mantled and exhumed terrains in Terra Meridiani, Mars, *J. Geophys. Res.*, *108*(E12), 8073, doi:10.1029/2002JE001982.

Boynton, W. V., et al. (2002), Distribution of hydrogen in the near surface of Mars: Evidence for subsurface ice deposits, *Science*, *297*, 81–85.

Byrne, S., and B. C. Murray (2002), North polar stratigraphy and the paleoerg of Mars, *J. Geophys. Res.*, *107*(E6), 5044, doi:10.1029/2001JE001615.

Campbell, B. A., and M. K. Shepard (2003), Coherent and incoherent components in near-nadir radar scattering: Applications to radar sounding of Mars, *J. Geophys. Res.*, *108*(E12), 5132, doi:10.1029/2003JE002164.

Fishbaugh, K. E., and J. W. I. Head (2005), Origin and characteristics of the Mars north polar basal unit and implications for polar geologic history, *Icarus*, *174*, 444–474.

Ford, P. G., and G. H. Pettengill (1992), Venus topography and kilometer-scale slopes, *J. Geophys. Res.*, *97*, 13,103–13,114.

Frey, H. V., J. H. Roark, K. M. Shockey, E. L. Frey, and S. E. H. Sakimoto (2002), Ancient lowlands on Mars, *Geophys. Res. Lett.*, *29*(10), 1384, doi:10.1029/2001GL013832.

Gendrin, A., et al. (2005), Sulfates in Martian layered terrains: The OMEGA/Mars Express view, *Science*, *307*, 1587–1591.

Hagfors, T. (1964), Backscattering from an undulating surface with application to radar returns from the Moon, *J. Geophys. Res.*, *69*, 3779–3784.

Holt, J. W., D. D. Blankenship, D. L. Morse, D. A. Young, M. E. Peters, S. D. Kempf, T. G. Richter, D. G. Vaughan, and H. F. J. Corr (2006a), New boundary conditions for the West Antarctic Ice Sheet: Subglacial topography of the Thwaites and Smith glacier catchments, *Geophys. Res. Lett.*, *33*, L09502, doi:10.1029/2005GL025561.

Holt, J. W., M. E. Peters, S. D. Kempf, D. L. Morse, and D. D. Blankenship (2006b), Echo source discrimination in single-pass airborne radar sounding data from the Dry Valleys, Antarctica: Implications for orbital sounding of Mars, *J. Geophys. Res.*, *111*, E06S24, doi:10.1029/2005JE002525.

Hynek, B. M. (2004), Implications for hydrologic processes on Mars from extensive bedrock outcrops throughout Terra Meridiani, *Nature*, *431*, 156–159.

Hynek, B. M., R. E. Arvidson, and R. J. Phillips (2002), Geologic setting and origin of Terra Meridiani hematite deposit on Mars, *J. Geophys. Res.*, *107*(E10), 5088, doi:10.1029/2002JE001891.

Ivanov, A. B., A. Safaeinili, G. Picardi, and J. J. Plaut (2006), Observations of the "Stealth" radar feature in the Mars Express MARSIS investigation, *Lunar Planet. Sci.* [CD-ROM], *XXXVII*, Abstract 1946.

Mellon, M. T., and B. M. Jakosky (1995), The distribution and behavior of Martian ground ice during past and present epochs, *J. Geophys. Res.*, *100*, 11,781–11,799.

Mellon, M. T., W. C. Feldman, and T. H. Prettyman (2004), The presence and stability of ground ice in the southern hemisphere of Mars, *Icarus*, *169*, 324–340.

Nunes, D. C., and R. J. Phillips (2006), Radar subsurface mapping of the polar layered deposits on Mars, *J. Geophys. Res.*, *111*, E06S21, doi:10.1029/2005JE002609.

Nunes, D. C., et al. (2006), Resolving stratigraphy of the polar layered deposits with MARSIS and SHARAD, *Lunar Planet. Sci.* [CD-ROM], *XXXVII* Abstract 1450.

Peeples, W. J., W. R. Sill, T. W. May, S. H. Ward, R. J. Phillips, R. L. Jordan, E. A. Abbott, and T. J. Killpack (1978), Orbital radar evidence for lunar subsurface layering in Maria Serenitatis and Crisium, *J. Geophys. Res.*, *83*, 3459–3468.

Phillips, R. J., et al. (1973), Apollo Lunar Sounder Experiment, in *Apollo 17 Preliminary Science Report*, *NASA Spec. Publ., NASA SP-330*, 22:1–22:26.

Picardi, G., et al. (2004), MARSIS: Mars Advanced Radar for Subsurface and Ionosphere Sounding, in *Mars Express: A European Mission to the Red Planet*, *Eur. Space Agency Spec. Publ., ESA SP-1240*, 51–69.

Picardi, G., et al. (2005), Radar soundings of the subsurface of Mars, *Science*, *310*, 1925–1928.

Planetary Data System (PDS) (2003), Planetary Data System Standards Reference, *Doc. JPL D-7669*, Part 2, Version 3.6, Jet Propul. Lab., Calif. Inst. of Technol., Pasadena.

Plaut, J. J., et al. (2006), MARSIS subsurface sounding observations of the South Polar Layered Deposits of Mars, *Lunar Planet. Sci.* [CD-ROM], *XXXVII*, Abstract 1212.

Putzig, N. E., et al. (2004), Mars thermal inertia from THEMIS data, *Lunar Planet. Sci.* [CD-ROM], *XXXV*, Abstract 1863.

Seu, R., et al. (2004), SHARAD: The MRO 2005 shallow radar, *Planet. Space Sci.*, *52*, 157–166.

Shchuko, O. B., D. V. Kartashov, G. Picardi, and R. Orosei (2003), Martian underground water detection: Thermal model and simulations of radar signal propagation, *J. Geophys. Res.*, *108*(E4), 8022, doi:10.1029/2002JE001879.

Squyres, S. W., et al. (2004), The Opportunity rover's Athena science investigation at Meridiani Planum,Mars, *Science*, *306*, 1698–1703.

Watters, T. R., C. J. Leuschen, J. J. Plaut, G. Picardi, A. Safaeinili, S. M. Clifford, W. M. Farrell, A. B. Ivanov, R. J. Phillips, and E. R. Stofan (2006), MARSIS radar sounder evidence of buried basins in the northern lowlands of Mars, *Nature*, *444*, 905–908, doi:10.1038/nature05356.

Zurek, R. W., and S. E. Smrekar (2007), An overview of the Mars Reconnaissance Orbiter (MRO) science mission, *J. Geophys. Res.*, doi:10.1029/2006JE002701, in press.

D. Biccari, A. Masdea, G. Picardi, and R. Seu, INFOCOM, Università di Roma "La Sapienza," Via Eudossiana 18, I-00184 Rome, Italy.

B. A. Campbell, Center for Earth and Planetary Studies, Smithsonian Institution, MRC 315, P.O. Box 37012, Washington, DC 20013, USA.

L. Marinangeli, IRSPS, Università G. d'Annunzio, Viale Pindaro 42, I-65127 Pescara, Italy.

D. C. Nunes, Lunar and Planetary Institute, 3600 Bay Area Boulevard, Houston, TX 77058, USA.

R. Orosei, Istituto di Astrofisica Spaziale e Fisica Cosmica, Rome, Italy.

R. J. Phillips, Department of Earth and Planetary Sciences, Washington University, Campus Box 1169, 1 Brookings Drive, St. Louis, MO 63130, USA. (phillips@wustite.wustl.edu)

J. J. Plaut, A. Safaeinili, and S. E. Smrekar, Jet Propulsion Laboratory, Mail Stop 183-501, 4800 Oak Grove Drive, Pasadena, CA 91109, USA.